

# **Karman constant and accurate mean flow prediction in a turbulent pipe**

Authors: Zhen-Su She\*<sup>1</sup>, Xi Chen<sup>1</sup>, You Wu<sup>1</sup>, Fazle Hussain<sup>1,2</sup>

*Affiliations:*

<sup>1</sup>*State Key Laboratory for Turbulence and Complex Systems and Department of Mechanics, College of Engineering, Peking University, Beijing, 100871, China*

<sup>2</sup>*Department of Mechanical Engineering, University of Houston, Houston, TX, 77204-4006, USA*

\* *Email address: she@pku.edu.cn*

# 1 **Summary**

2 The Karman constant  $\kappa$  - widely used in atmospheric science and engineering  
3 turbulence modelling, and proposed by Prandtl<sup>1</sup> in 1925 and von Karman<sup>2</sup> in 1930 to  
4 describe the mean velocity of a turbulent wall-bounded flow<sup>3</sup> - leads to a logarithmic  
5 profile in an overlap region near the wall. For over eighty years, its value was believed  
6 to be  $\sim 0.41$ . But more recently, many argue that it is not a constant, because of  
7 measured variations in different flows and at different Reynolds numbers  $(Re)^{4-6}$ . Here,  
8 a multi-layer analytic theory<sup>7</sup> is shown to lead to a re-interpretation of  $\kappa$  as a global  
9 constant for both the overlap region and outer flow, and to yield a new method for its  
10 measurement. The newly determined value is 0.45 for both channel and pipe. It is  
11 shown that this new  $\kappa$ , together with other wall constants, yields a 99% accuracy in the  
12 prediction of mean velocity data at *all points* in high  $Re$  (up to 40 million) pipe flow.  
13 The theory also describes finite  $Re$  effect, and discovers a transition at the friction  $Re$   
14 (i.e.  $Re_{\tau} = 5000$ ). An accurate model for the prediction of turbulent transport in  
15 canonical pipe and channel flows is achieved here, and we propose the model to be  
16 valid for a wide class of turbulent flows.

17

## 18 **Text**

19       Accurate prediction of turbulent flow remains a top challenge in classical physics.  
20 Even for simple wall-bounded flows such as pipe and channel, analytic prediction of  
21 mean velocities at very high  $Re$  relies on empirical functions<sup>8</sup> with compromised  
22 accuracy, and continues to receive vivid attention with great experimental efforts<sup>9-14</sup>.  
23 Deriving a mean-field prediction based on first principles is highly desired, as it would  
24 reveal new statistical symmetries governing turbulent fluctuations and allow a deeper  
25 understanding of important constants describing the flow.

26       Prandtl<sup>1</sup> in 1925, and von Karman<sup>2</sup> in 1930, independently suggested the concept of  
27 *mixing length* - analogous to the mean free path for molecular collisions - to model  
28 turbulent transport. A simple model of the mixing length with linear dependence on the  
29 distance from the wall yields a logarithmic mean velocity profile (MVP), where a  
30 proportionality constant - the Karman constant  $\kappa$  - was introduced. However, this  
31 empirical model has led to controversies: Barenblatt and co-authors<sup>15-16</sup> have claimed  
32 that power-law is a better description. Indeed, theoretical interpretation of the log-law is  
33 very unsatisfactory. For example, very little is understood about  $\kappa$  and the other log-law  
34 constant  $B$ ; their variability with different flows and different  $Re$  remains elusive<sup>4-6</sup>.  
35 While the log-law vs. power law debate is still vivid<sup>17-18</sup>, we present a coveted theory  
36 which re-interprets  $\kappa$  with a new method for its measurement. Not only a more  
37 accurate description of the entire MVP over a wide range of  $Re$  is obtained, the theory  
38 also predicts, for the first time, a critical  $Re$  in Princeton pipe experiment, and derives  
39 quantities of engineering interest. The theory presented here provides a general guide

40 for accurate mean-field prediction from post-analysis of massive simulation data for a  
41 wide class of turbulent flows.

42 The mean velocity in a turbulent pipe flow has resisted analytic attack since the turn  
43 of the last century<sup>9</sup>. We overcome this bottleneck by developing a symmetry analysis on  
44 the mean momentum equation (MME), utilizing empirical knowledge about the  
45 multiple layers. For a channel or a pipe, the MME has an exact first-integral<sup>19</sup>, written  
46 in wall units as

47 
$$S^+ + W^+ = 1 - y^+ / \text{Re}_\tau = r, \quad (1)$$

48 where  $S^+ = dU^+ / dy^+$  is the mean shear and  $W^+ = -\langle u'v' \rangle^+$  is the Reynolds stress,  
49 and  $y^+$  the distance to the wall,  $r$  the distance to the center,  $\text{Re}_\tau$  the friction Reynolds  
50 number, and  $+$  denotes normalization using wall units. Our symmetry analysis involves  
51 a length determined by the two primary variables,  $W^+$  and  $S^+$ , which is, by  
52 dimensional argument,  $\ell_M^+ = \sqrt{W^+} / S^+$ . This length is regarded<sup>7</sup> as an “order  
53 parameter” used to represent effects of fluctuations in statistical mean-field theory<sup>20</sup>,  
54 and happens to coincide with the mixing length<sup>1,2</sup> for describing the vertical mean  
55 momentum transport. The concept of length order parameter is more general, however,  
56 and is applicable to analyze other flows.

57 The symmetry analysis of the multi-layer structure is accomplished by a Lie-group  
58 theory<sup>7</sup> which derives the entire profile of the mixing length in two steps: First, identify  
59 local invariant solutions for each of the layers: well known as sublayer, buffer layer,  
60 bulk zone, and a new central zone called ‘core’. Each of the layers is postulated to  
61 possess a local scaling for the mixing length or its gradient under the dilation

62 transformation. Then, the theory<sup>7</sup> postulates a transition ansatz and derives a combined,  
 63 analytic expression for the entire profile of the mixing length:

$$64 \quad \ell_M^+ = \rho \left( \frac{y^+}{y_{sub}^+} \right)^{3/2} \left( 1 + \left( \frac{y^+}{y_{sub}^+} \right)^{p_I} \right)^{1/(2p_I)} \left( 1 + \left( \frac{y^+}{y_{buf}^+} \right)^{p_{II}} \right)^{-1/p_{II}} \frac{1-r^m}{m(1-r)Z_{core}} \left( 1 + \left( \frac{r}{r_{core}} \right)^{-p_{IV}} \right)^{1/(2p_{IV})}. \quad (2)$$

65 This determines the mean shear profile<sup>19</sup>

$$66 \quad S^+ = (-1 + \sqrt{4r\ell_M^{+2} + 1}) / (2\ell_M^{+2}), \quad (3)$$

67 hence the mean velocity profile  $U^+ = \int S^+ dy^+$ , the average velocities

$$68 \quad (\overline{U^+}^{Pipe} = 2 \int U^+ r dr \text{ and } \overline{U^+}^{CH} = \int U^+ dr), \text{ and the friction factor } C_f = 8 / \overline{U^+}^2. \text{ While}$$

69 previous work reported heuristic and systematic derivation<sup>7</sup> of Eq.(2), the main task  
 70 here is to determine the parameters with a systematic method, and to demonstrate that  
 71 the Karman constant is indeed a constant, and that there is a transition at  $Re_\tau = 5000$ .

72 Two sets of parameters appear in Eq.(2). The *first* are four coefficients:

73  $\rho, y_{sub}^+, y_{buf}^+, r_{core}$ ; the *second* are called transition sharpnesses:  $p_I, p_{II}, p_{IV}$ , which  
 74 describe the transition between sublayer and buffer, buffer and log region, and bulk and  
 75 core. The second set, less sensitive to the predictions, are chosen to be integers  
 76 ( $p_I = p_{II} = 4, p_{IV} = 2$ ). We focus below on the determination of the four coefficients.

77 First, the inner solution near the wall determines  $\rho$  and  $y_{sub}^+$ . From Eq.(2), we

78 find that for  $y^+ \ll y_{sub}^+, \ell_M^+ \approx \rho (y^+ / y_{sub}^+)^{3/2}$ . If the local scaling exists,

79  $\ell_M^+ / y^{+3/2} \approx \rho (y_{sub}^+)^{-3/2}$  is a constant near the wall, determined by  $\rho$  and  $y_{sub}^+$ . Fig.1

80 shows that well resolved direct numerical simulation (DNS) data for channel flow  
 81 indeed confirms the existence of the constant, with a value of 0.0315. In order to

82 determine  $y_{sub}^+$ , note that it is the location where the local scaling is in the middle of 3/2  
83 (sublayer scaling) and 2 (buffer scaling); thus,  $d \ln \ell_M^+ / d \ln y^+ |_{y_{sub}^+} = (1+3/2)/2 = 7/4$ .  
84 Furthermore, we assume, with accurate empirical support from DNS data, that this  
85 transition point coincides with the maximum of  $\Gamma = S^+ y^+$ , the diagnostic function used  
86 to quantify near-wall statistics<sup>4</sup>. With the assumption  $d\Gamma(y_{sub}^+)/dy^+ = 0$ , we  
87 differentiate Eq.(1) at  $y^+ = y_{sub}^+$  to derive the following appealing results:  
88  $S^+(y_{sub}^+) = 3/5$ ,  $W^+(y_{sub}^+) = 2/5$ ,  $\ell_M^+(y_{sub}^+) = \sqrt{10}/3$ . This yields the prediction:  
89  $\rho_0 \approx 2^{3/8} \sqrt{5}/3 \approx 0.967$ ; then, using the above empirical near-wall measurement, we  
90 obtain  $y_{sub}^+ \approx 9.80$ .

91 Next, Eq.(2) predicts an analytic scaling function for the mean defect velocity (i.e.  
92 difference from the centreline velocity  $U_c^+$ ) (see Fig.2). Fig.2a confirms this linear  
93 relation for channel (DNS) and pipe (Princeton data) over a wide range of  $Re$  (a  
94 complete collapse); then,  $\kappa$  is derived from the slope with high accuracy. Fig.2b  
95 shows a procedure for the determination of  $r_{core}$ . A conservative estimate of the  
96 Karman constant is  $\kappa \approx 0.45 \pm 0.014$ ; the measured  $r_{core}$  for Princeton pipe data is  
97  $r_{core}^{(\infty)} \approx 0.67 \pm 0.3$ , which is believed to be the asymptotic value at high  $Re$ . From the  
98 matching condition,  $\kappa = \rho y_{buf}^+ / y_{sub}^{+2}$ , we obtain  $y_{buf}^{+(\infty)} \approx 44.7$ . Fig. 3 compares our  
99 predicted MVP with Princeton pipe data using these four parameter values, showing  
100 uniform agreement of the entire profile with 99% accuracy for  $Re$  up to forty million.  
101 This unprecedented accuracy, based on objectively measured physical parameters,  
102 supports that turbulence in pipe indeed admits an analytic solution!

103 Note, however, that the core-layer thickness for DNS channel data at moderate  $Re$   
104 (Fig.2b) shows notable difference from Princeton pipe data:  $r_{core}^{DNS} \approx 0.27$ . We attribute  
105 it to finite  $Re$  effect which can now be studied. Define  $r_{core}^{DNS} \approx r_{core}^{(\infty)}(1 - \varepsilon_c)$ , then  
106 departure at DNS  $Re$  ( $Re_\tau \approx 10^3$ ) gives  $\varepsilon_c \approx 0.6$ . Furthermore, we believe that the  
107  $Re$ -effect in the bulk flow ( $r_{core}$ ) would influence the overlap region ( $y_{buf}^+$ ), leading to a  
108 change in  $\rho = \rho_0(1 + \varepsilon_\rho)$ . Fig.1(b) indeed shows evidence of such departure with  
109  $\varepsilon_\rho \approx 0.1$ , which yields a higher plateau of 0.035. The  $Re$ -effect is further validated by  
110 the measured centreline velocity  $U_c^+$  and average velocity  $\overline{U}^+$ , and skin friction  
111 coefficient  $C_f$  derived from Eq.(2) (see the Method). Fig.3b, using a compensated  
112 plot against asymptotic high  $Re$  result, shows clearly that a transition takes place around  
113  $Re_\tau^{(crit)} \approx 5000$ . Furthermore, a simple model for linear dependence of  $\varepsilon_\rho$  and  $\varepsilon_c$  on  
114  $Re$  below  $Re_\tau^{(crit)}$  yields an accurate description of friction coefficients for all pipe data.

115 The theory also derives several empirical constants of engineering interest. A  
116  $Re$ -independent quantity for pipe can be predicted:  $(U_c^+ - \overline{U}^+)^{Pipe} \approx 4.3$ , which is very  
117 close to the empirical value (see Fig.3b), improving Pope's derivation<sup>3</sup>, i.e.  $1.5/\kappa$  (3.3,  
118 using  $\kappa \approx 0.45$ ). Furthermore, we derive a new formula for turbulent pipe for a widely  
119 useful relation between  $Re_\tau$  and  $Re$ : our result,  $Re_\tau \approx 0.26 Re / \ln Re$ , should replace  
120 the popular empirical formula<sup>3</sup>:  $Re_\tau \approx 0.09 Re^{0.88}$ . The latter has an error of up to 25%  
121 at  $Re_\tau = 5 \times 10^5$  according to Princeton data; ours is less than 1%. We also predict a

122 constant difference of centreline velocity between channel and pipe:

123  $U_c^{+Pipe} - U_c^{+CH} \approx 1.1$ , in sharp contrast to [19] which predicts a notable  $Re$ -dependence.

124 In summary, we have achieved an accurate description of turbulent mean velocity,

125 which differentiates the effect of geometry (pipe versus channel) with a single integer

126 ( $m=5$  versus  $m=4$ ), and identified four physical parameters which are *not* fitting

127 parameters, but measured systematically from accurate experimental/numerical data.

128 We obtain also the first theory which predicts finite  $Re$  effect, and discovers a transition

129 at  $Re_\tau^{(crit)} \approx 5000$  for the friction factor. The most notable outcome is the universality of

130  $\kappa$ ; it resets the status of the Karman constant to be intimately related to universal

131 small-scale dynamics of fully developed bulk flow turbulence, even possibly to the

132 Kolmogorov constant<sup>24</sup>.

133 The conceptual framework developed here is encompassing and goes far beyond

134 the classical mixing length theory, as the mixing length is used here to reveal the

135 *complete* multi-layer structure which is a general feature of a wide class of

136 wall-bounded turbulent flows. We also show a procedure for extracting quantitative

137 information from empirical data, which can be adapted to a variety of turbulent flows.

138 Indeed, the analysis has been successfully extended to incompressible, compressible

139 and rough-wall turbulent boundary layers, and our results will soon be communicated.

140 Another interesting application underway is turbulent Rayleigh-Benard convection<sup>25</sup>;

141 the mean profiles (of velocity and temperature) can now be quantitatively described by

142 a symmetry study of the mixing length and one or more order functions associated with

143 temperature fluctuations.

144

145 **Method**

146 Analytic expressions for mean velocities can be derived from Eq.(2), to yield a  
 147 systematic procedure for determining four physical model parameters. In the outer  
 148 region, Eq.(1) yields:  $dU^+ / dr \approx -\sqrt{r} / \ell_M$ . Then, using Eq.(2) for  $y^+ \gg y_{buf}^+$ :

149 
$$U^{+(Outer)}(r) = U^+(0) - \frac{1}{\kappa} f(r, r_{core}) = U_c^+ - \frac{m}{\kappa} Z_{core} \int_0^r \frac{r' dr'}{(1-r'^m)(r'^2+r_{core}^2)^{1/4}}, \quad (4)$$

150 where  $f(r, r_{core})$  characterizes the bulk mean flow and depends only on one parameter:  
 151  $r_{core}$ . Once  $r_{core}$  is specified, it is a simple least-squares problem to derive optimal  
 152 values of  $\kappa$  and  $U_c^+$  from a set of measured mean velocities,  $U^{+EXP}(r_i)$ . The  
 153 determination of  $r_{core}$  is realized using the relative error function,

154 
$$\sigma_U = \frac{1}{N} \sum (1 - U^+(r_i) / U^{+EXP}(r_i))^2$$
, which measures how close the function  $f(r, r_{core})$

155 describes the real data  $U^{+EXP}(r_i)$ . Note  $r_{core}$  and  $\kappa$  are determined by independent  
 156 criteria. The validity of the method is clearly demonstrated in Fig.2.

157 Analysis of empirical data shows that both  $r_{core}$  and  $\rho$  have notable  
 158  $Re$ -dependence, while  $\kappa$  and  $y_{sub}^+$  are remarkably universal. To further elaborate on  
 159 this, analytic expression for the centreline velocity is derived below. Let us write:

160 
$$U_c^+(Re_\tau) = U_{buf}^+ + \Delta U_{bulk}^+ + \Delta U_{core}^+ \approx \int_0^{y_{buf}^+} \frac{-1 + \sqrt{4\ell_M^{+2} + 1}}{2\ell_M^{+2}} dy^+ + \left( \int_{y_{buf}^+}^{y_{core}^+} + \int_{y_{core}^+}^{Re_\tau} \right) \frac{\sqrt{r}}{\ell_M^+} dy^+, \quad (5)$$

161 where the near-wall contribution is expressed by  $U_{buf}^+ = U^+(y_{buf}^+)$ , the bulk by  $\Delta U_{bulk}^+$ ,  
 162 and the core layer by  $\Delta U_{core}^+$ , with  $y_{core}^+ = (1 - r_{core}) Re_\tau$ . Finite  $Re$  effect is described by  
 163 two small parameters,  $\varepsilon_\rho$  and  $\varepsilon_c$ , defined as  $\rho = \rho_0(1 + \varepsilon_\rho)$  (hence

164  $y_{buf}^+ = y_{buf}^{+(\infty)}(1 - \varepsilon_\rho)$  and  $r_{core} = r_{core}^{(\infty)}(1 - \varepsilon_c)$ . A perturbation analysis yields:

165  $U_{buf}^+(\varepsilon_\rho) \approx y_{buf}^{+(\infty)}(0.33 - 0.20\varepsilon_\rho)$ . Substitute  $\ell_M^{(bulk)} \approx \kappa(1 - r^m)/m$  into (6), to obtain

166  $\Delta U_{bulk}^+ \approx [\ln(y_{core}^+ / y_{buf}^+) + \Lambda(r_{core})] / \kappa$ , where  $\Lambda(r) = \psi(r_{buf}) - \psi(r)$  ( $r_{buf} = 1 - y_{buf}^+ / \text{Re}_\tau \approx 1$

167 for high  $Re$ ) and  $\psi(r)$  has an analytic expression [26]. Next, substitute

168  $\ell_M^{(core)} \approx \kappa(1 + (r_{core}/r)^2)^{1/4} / (5Z_{core})$  into (6), to obtain  $\Delta U_{core}^+ \approx 5Z_{core} r_{core}^{3/2} / (2\kappa)$ . Summarizing

169 all the terms above, we obtain a first-order approximation for the centreline velocity:

$$170 \quad U_c^{+Pipe(CH)} \approx U_c^{+Pipe(CH)(\infty)} - 6.72\varepsilon_\rho + 1.51(1.68)\varepsilon_c \quad (6)$$

171 where  $U_c^{+Pipe(CH)(\infty)} \approx \ln(\text{Re}_\tau) / \kappa + 8.37(7.28)$ . This yields, for the first time, the centreline

172 velocity difference between a pipe and a channel at the same  $Re$ :

173  $U_c^{+Pipe} - U_c^{+CH} \approx 1.09 - 0.17\varepsilon_c$ . Finally, the average velocities also have an analytic

174 expression:

$$175 \quad \overline{U}^{+Pipe(CH)} \approx \overline{U}^{+Pipe(CH)(\infty)} - 6.84\varepsilon_\rho + 0.26(0.36)\varepsilon_c. \quad (7)$$

176 where  $\overline{U}^{+Pipe(CH)(\infty)} \approx \ln(\text{Re}_\tau) / \kappa + 4.1(5.0)$ . This allows an evaluation of the bulk velocity

177 Reynolds number in pipe:  $\text{Re} = \overline{2U} / \nu = 2\overline{U}^+ \text{Re}_\tau$ , and friction coefficient:

$$178 \quad C_f^{Pipe} = 8 \left( \overline{U}^{+Pipe} \right)^{-2} \approx C_f^{Pipe(\infty)} [1 + (13.68\varepsilon_\rho - 0.52\varepsilon_c) \sqrt{C_f^{Pipe(\infty)} / 8}]. \quad (8)$$

179 where  $C_f^{Pipe(\infty)} = 8 \left( \overline{U}^{+Pipe(\infty)} \right)^{-2}$ . A simple linear model for  $\varepsilon_{\rho(c)}$  is introduced as:

$$180 \quad \varepsilon_{\rho(c)} = \varepsilon_{\rho(c)}^{(0)} (\text{Re}_\tau^{(crit)} - \text{Re}_\tau) / (\text{Re}_\tau^{(crit)} - 1000), \quad (9)$$

181 where  $\varepsilon_\rho^{(0)} \approx 0.1$  and  $\varepsilon_c^{(0)} \approx 0.6$  are derived from empirical data.

182

## 183 **References**

- 184 1. Prandtl, On fluid motions with very small friction (in German). *Third International*  
185 *Mathematical Congress*. Heidelberg, 484–491 (1904).
- 186 2. von Karman, T. Mechanische Ahnlichkeit und Turbulenz. In *Proc. Third Int. Congr.*  
187 *Applied Mechanics*, Stockholm. 85-105 (1930).
- 188 3. Pope, S.B. *Turbulent flows*. 264-295 (Cambridge University Press, 2000).
- 189 4. Smits A. J., McKeon B. J., Marusic I., High Reynolds number wall turbulence.  
190 *Annu. Rev. Fluid Mech.* 43:353-75 (2011).
- 191 5. Nagib, H.M. and Chauhan, K.A. Variations of von Kármán coefficient in canonical  
192 flows. *Phys. Fluids*. **20**, 101518 (2008).
- 193 6. Marusic, I., *et al.* Wall-bounded turbulent flows at high Reynolds numbers: Recent  
194 advances and key issues. *Phys. Fluids*. **22**, 065103 (2010).
- 195 7. She, Z.S., Chen, X., Wu, Y. and Hussain, F. New perspectives in statistical  
196 modeling of wall-bounded turbulence. *Acta Mechanica Sinica*. **26**, 847-861 (2010);  
197 She, Z.S., Chen, X. and Hussain, F. A Lie-group derivation of a multi-layer mixing  
198 length formula for turbulent channel and pipe flows. *Submitted JFM fast track*  
199 (2011); see also Supplementary information.
- 200 8. Wilcox, D.C. *Turbulence Modeling for CFD*. (DCW Industries, 2006), 181-182.
- 201 9. Reynolds, O. An experimental investigation of the circumstances which determine  
202 whether the motion of water shall be direct or sinuous, and the law of resistance in  
203 parallel channels. *Phil. Trans. R. Soc. London, Ser. A*. **174**, 935-982 (1883).
- 204 10. Zagarola, M.V. and Smits, A.J. Scaling of the mean velocity profile for turbulent  
205 pipe flow. *Phys. Rev. Lett.* **78**, 239-242 (1997).

- 206 11. Swanson, C., Julian B., Ihas, G.G. and Donnelly, R., Pipe flow measurements over a  
207 wide range of Reynolds numbers using liquid helium and various gases, *J. Fluid*  
208 *Mech.* 461, 51-60 (2002).
- 209 12. Zanon, E.S., Durst, F. and Nagib, H. Evaluating the law of the wall in  
210 two-dimensional fully developed turbulent channel flows. *Phys. Fluids.* **15**,  
211 3079-3089 (2003).
- 212 13. B. J. McKeon, J. Li, W. Jiang, J. F. Morrison, and A. J. Smits. *J. Fluid Mech.* **501**,  
213 135 (2004); the data are available at [http://gasdyn.princeton.edu/data/e248/mckeon\\_](http://gasdyn.princeton.edu/data/e248/mckeon_data.html)  
214 [data.html](http://gasdyn.princeton.edu/data/e248/mckeon_data.html).
- 215 14. Talamelli, A. *et al.* CICLOPE—a response to the need for high Reynolds number  
216 experiments. *Fluid Dyn. Res.* **41**, 021407 (2009).
- 217 15. Barenblatt, G.I. Scaling laws for fully developed turbulent shear flows. Part 1. Basic  
218 hypotheses and analysis. *J. Fluid Mech.* **248**, 521-529 (1993).
- 219 16. Barenblatt, G.I., Chorin, A.J. and Prostokishin V.M. Scaling laws for fully  
220 developed turbulent flow in pipes: Discussion of experimental data. *Proc. Natl.*  
221 *Acad. Sci.* 94, 773-776 (1997).
- 222 17. Zagarola, M.V., Perry, A.E. and Smits, A.J. Log laws or power laws: The scaling in  
223 the overlap region. *Phys. Fluids.* **9**, 2094-2100 (1997).
- 224 18. George, W.K. Is there a universal log-law for turbulent wall-bounded flow? *Phil.*  
225 *Trans. R. Soc. London, Ser. A.* **365**, 789-806 (2007).
- 226 19. L'vov, V.S., Procaccia, I. and Rudenko, O. Universal model of finite Reynolds  
227 number turbulent flow in channels and pipes. *Phys. Rev. Lett.* **100**, 050504 (2008).
- 228 20. Kadanoff, L. P. More is the same; phase transitions and mean field theories. *J. Stat.*  
229 *Phys.* **137**, 777–797 (2009).

- 230 21. Iwamoto, K., Suzuki, Y. and Kasagi, N. Database of fully developed channel flow.  
 231 *THTLAB Internal Report*. No. ILR-0201 (2002).
- 232 22. Hoyas, S. and Jimenez, J. Scaling of the velocity fluctuations in turbulent channels  
 233 up to  $Re_{\tau} = 2003$ . *Phys. Fluids*. **18**, 011702 (2006).
- 234 23. Wu, X.H. and Moin, P. A direct numerical simulation study on the mean velocity  
 235 characteristics in turbulent pipe flow. *J. Fluid Mech.* **608**, 81-112 (2008).
- 236 24. Lo, T.S., L'vov, V.S., Pomyalov A. and Procaccia, I. Estimating von-Karman's  
 237 constant from homogeneous turbulence. *Europhys. Lett.* **72**, 943 (2005).
- 238 25. Ahlers, G., Grossmann, S. and Lohse, D. Heat transfer and large scale dynamics in  
 239 turbulent Rayleigh-Bénard convection. *Rev. Mod. Phys.* **81**, 503–537 (2009).
- 240 26. For pipe flow ( $m=5$ ), the explicit form is

241 
$$\psi^{Pipe}(r) = 2\ln(1+\sqrt{r}) + \frac{\sqrt{5}-1}{4}\ln\varphi^+(r) + \frac{\sqrt{5}+1}{4}\ln\varphi^-(r) + \frac{2\sqrt{5}}{c^-}\arctan\frac{c^-\sqrt{r}}{A^-(r)} - \frac{2\sqrt{5}}{c^+}\arctan\frac{c^+\sqrt{r}}{A^-(r)},$$
 where

242 
$$\varphi^+(r) = \frac{A^+(r)-B^+(r)}{A^+(r)+B^+(r)}, \quad \varphi^-(r) = \frac{A^+(r)-B^-(r)}{A^+(r)+B^-(r)}, \quad A^+(r) = 2(1+r); \quad A^-(r) = 2(1-r);$$

243 
$$B^+(r) = (\sqrt{5}+1)r; \quad B^-(r) = (\sqrt{5}-1)r; \quad c^+ = \sqrt{10+2\sqrt{5}}; \quad c^- = \sqrt{10-2\sqrt{5}}.$$

244

## 245 End Notes

246

247 **Acknowledgements** We thank G. Ahlers, E. Bodenschatch, N. Goldenfeld, H.  
 248 Swinney for helpful discussions. This work was supported by the National Natural  
 249 Science Foundation of China (90716008 and 10921202), MOST 973 Project  
 250 (2009CB724100). Part of the work was completed during our visit at KITP of UCSB  
 251 during “Turbulence program”, supported by the National Science Foundation of US

252 under Grant No. NSF PHY05-51164, which is gratefully acknowledged.

253

254 **Author Contribution**

255 Z.S.S. established the theoretical framework, and directed the research in collaboration  
256 with F.H., X.C. and Z.S.S. developed the analysis, and X.C. measured the physical  
257 constants. Y.W. performed quantitative study of the model and compared the  
258 predictions with the empirical data. Z.S.S., X.C. and F.H. wrote the manuscript. All  
259 authors extensively discussed the results and interpretations, and commented on the  
260 manuscript.

261

262 **Author Information** The authors declare no competing financial interests.

263 Correspondence and requests for materials should be addressed to Z.S.S.  
264 (she@pku.edu.cn).

265

266

## 267 **Figure Legends**

268 **Figure 1.** Validation of the multi-layer description of the mixing length profile and the  
269 determination of the near-wall constants. Three sets of best resolved DNS data are used:  
270 two channel flows from Iwamoto *et al.*<sup>21</sup> at  $Re_\tau \approx 650$  (black circles) and Hoyas and  
271 Jimenez<sup>22</sup> at  $Re_\tau \approx 940$  (black squares), and one pipe flow of Wu and Moin<sup>23</sup>  
272 at  $Re_\tau \approx 1142$  (blue triangles). (a): Compensated plot of the mixing length,  
273  $\ell_M^{DNS} / (1 - r^m)$ , illustrates four layers: sublayer, buffer, log-bulk and core. Two plateaus  
274 ( $m = 4$  for channel and  $m = 5$  for pipe) illustrate the bulk flow structure, with the  
275 same  $\kappa = 0.45$ . The solid lines are predictions of Eq.(1) using the measured  $\kappa$  and  
276 other parameters. (b): Near-wall behaviour compared to theoretical prediction,  
277  $\rho_0 / y_{sub}^{+3/2} \approx 0.0315$  (dashed line), finite- $Re$  description of composite solution (solid  
278 line), and corresponding buffer-layer description (dash-dotted line), which measure two  
279 constants. The functions<sup>7</sup>  $B^{s-b} = (1 + (y^+ / y_{sub}^+)^4)^{1/8}$  and  $B^{b-l} = (1 + (y^+ / y_{buf}^+)^4)^{-1/4}$ .

280

281 **Figure 2.** Determination of the Karman constant,  $\kappa$ , and the core-layer thickness,  
282  $r_{core}$ . (a) Plot of measured  $U_d^+(r) = U^+(0) - U^{+EXP}(r)$  versus theoretical function  
283  $f(r, \bar{r}_{core})$ , to illustrate a good linear relationship consistent with the measured universal  
284 constant  $\kappa \approx 0.45$ , for both channel and pipe flows for a wide range of  $Re$ . Inset shows  
285 the measurement for all Princeton data for  $Re_\tau > 5000$ . Star is the final measured value:  
286  $r_{core}^{-EXP} \approx 0.67$  for Princeton data at relatively high  $Re$ , while  $r_{core}^{-DNS} \approx 0.27$  for DNS data  
287 at moderate  $Re$ , and  $\kappa \approx 0.45$  in both cases. (b) Result of applying the procedure to

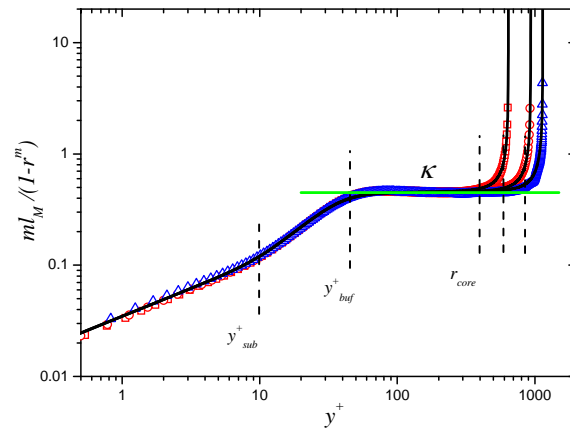
288 four sets of data: one theoretical profile generated from Eq.(1) and Eq.(2) to test the  
 289 validity of the procedure, second profile with noise added to the former to test the  
 290 robustness of the method, third profile from DNS channel simulation, and Princeton  
 291 pipe data<sup>13</sup>. Note that the DNS profile follows closely the same error variation pattern as  
 292 the theoretical profile, validating the theory with a clear determination of  $r_{core}$  and  
 293 yielding a reliable estimate of  $\kappa$  and  $U_c^+$ . On the other hand, the profile with small  
 294 random noise (0.5% ) yields an error variation pattern, closely resembling Princeton  
 295 pipe data, which yields a scatter (20-30%) of the estimated  $r_{core}$ , but a much smaller  
 296 uncertainty of  $\kappa$  (only 3%). This explains the scatter in the measured  $r_{core}$  presented  
 297 in the inset of (a), and the slight variation of  $\kappa$ .

298

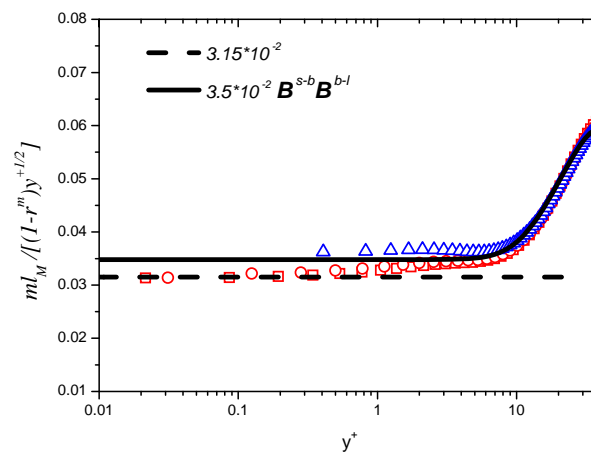
299 **Figure 3.** (a): Theoretical (solid lines) and measured MVPs, which are staggered  
 300 vertically by five units for clarity. Inset shows the relative errors,  
 301  $(U^{EXP} / U^{Theory} - 1) \times 100\%$ . Note that errors in our theoretical predictions (red solid  
 302 symbols) are uniformly within 1%. Also included is the recent model of L'vov,  
 303 Proccacia and Rudenko (LPR<sup>19</sup>) (blue open symbols) - the only other theoretical model  
 304 for entire MVP at finite  $Re$ . The LPR model has three adjustable parameters, the most  
 305 important choices being  $\kappa = 0.415$  for channel and 0.405 for pipe. It reveals  
 306 systematic deviations at high  $Re$ . (b): Compensated plot of friction coefficient  
 307  $C_f^{EXP} / C_f^{Pipe(\infty)}$  shows a transition around  $Re_{\tau}^{(crit)} = 5000$  (black dot line). The dash line  
 308 indicates  $C_f^{EXP} = C_f^{Pipe(\infty)}$ , and the dash-dot line is a linear finite  $Re$  model for both  $\varepsilon_{\rho}$   
 309 and  $\varepsilon_c$  given by Eq.(8) and (9). Inset compares the present prediction of

310  $(U_c^+ - \overline{U^+})^{Pipe} \approx 4.3$  (black dash line) to Princeton data (symbols), far improving previous  
311 description in [3] (blue solid line).

312 **Figure 1.**



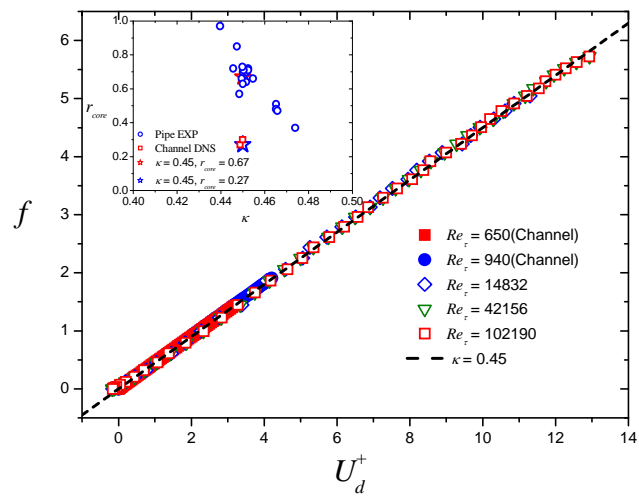
313



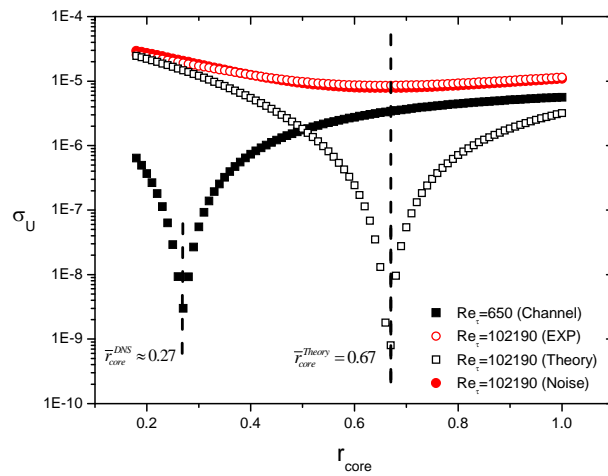
314

315

316 **Figure 2.**



317

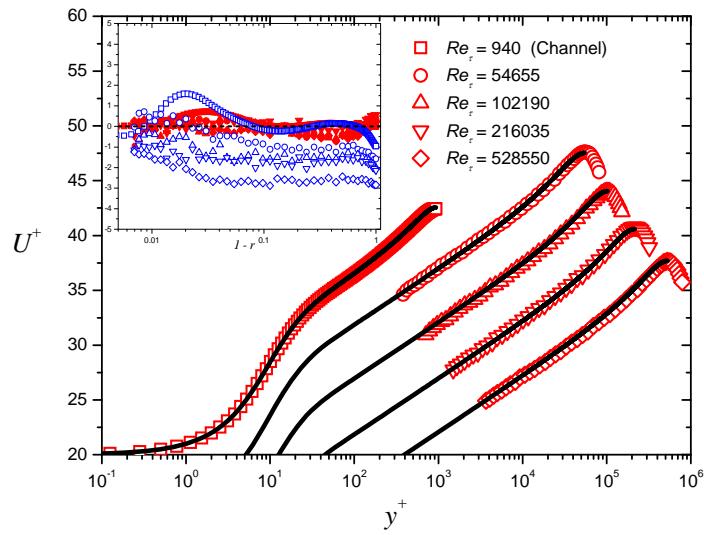


318

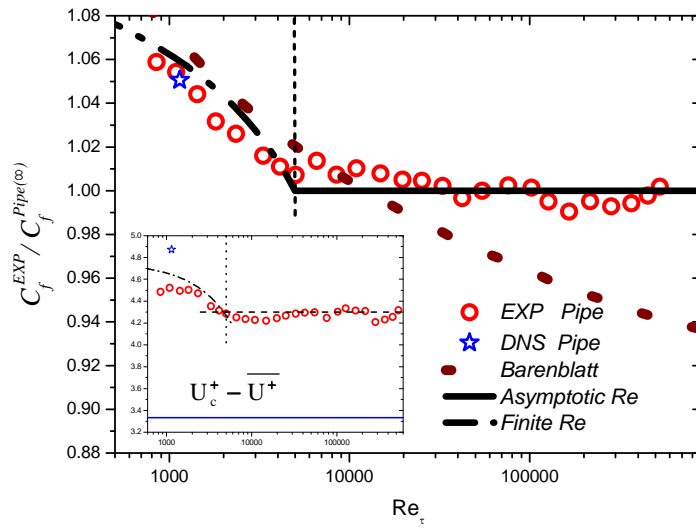
319

320

321 **Figure 3.**



322



323

324

325

326 **End**